On the Use of Radiosondes in Freezing Precipitation

SEAN WAUGH

NOAA/OAR/National Severe Storms Laboratory, and Cooperative Institute for Mesoscale Meteorological Studies, University of Oklahoma, Norman, Oklahoma

TERRY J. SCHUUR

Cooperative Institute for Mesoscale Meteorological Studies, University of Oklahoma, and NOAA/OAR/National Severe Storms Laboratory, Norman, Oklahoma

(Manuscript received 13 April 2017, in final form 4 January 2018)

ABSTRACT

Radiosonde observations are used the world over to provide critical upper-air observations of the lower atmosphere. These observations are susceptible to errors that must be mitigated or avoided when identified. One source of error not previously addressed is radiosonde icing in winter storms, which can affect forecasts, warning operations, and model initialization. Under certain conditions, ice can form on the radiosonde, leading to decreased response times and incorrect readings. Evidence of radiosonde icing is presented for a winter storm event in Norman, Oklahoma, on 24 November 2013. A special sounding that included a particle imager probe and a GoPro camera was flown into the system producing ice pellets. While the iced-over temperature sensor showed no evidence of an elevated melting layer (ML), complementary Particle Size, Image, and Velocity (PASIV) probe and polarimetric radar observations provide clear evidence that an ML was indeed present. Radiosonde icing can occur while passing through a layer of supercooled drops, such as frequently found in a subfreezing layer that often lies below the ML in winter storms. Events that have warmer/deeper MLs would likely melt any ice present off the radiosonde, minimizing radiosonde icing and allowing the ML to be detected. This paper discusses the hypothesis that the absence of an ML in the radiosonde data presented here is more likely to occur in winter storms that produce ice pellets, which tend to have cooler/shallower MLs. Where sounding data do appear to be compromised by icing, polarimetric radar data might be used to identify MLs for nowcasting purposes and numerical model initialization.

1. Introduction

Radiosondes are used the world over to provide fundamental observations throughout the depth of the lower atmosphere (Luers and Eskridge 1998). In the United States, National Weather Service (NWS) forecast offices across the country coordinate radiosonde launches of weather balloons twice a day (valid at 0000 and 1200 UTC) to obtain vertical profiles of the atmosphere that are used to produce local forecast products and initialize a variety of forecast models. During major severe or winter weather events, NWS offices also occasionally launch additional soundings to provide supplemental data to forecasters. While the majority of these radiosondes are launched in clear air, the timing of the launch occasionally requires measurements to be taken in precipitation or for the sounding to travel through cloud (Bosart and Nielsen 1993). In these situations, care must be taken to ensure that the sometimes harsh in-cloud environment does not impact the radiosonde data quality. This is particularly true for winter storms, where even small variations in the temperature profile at key levels of the atmosphere, such as in an elevated warm melting layer (ML) or a low-level cold refreezing layer, can determine whether a forecast calls for rain, freezing rain, ice pellets, or snow (e.g., Czys et al. 1996; Bourgouin 2000; Rauber et al. 2001; Kumjian et al. 2013; Reeves et al. 2014, 2016).

Given the sensitivity of the precipitation type forecast in winter storms to the vertical temperature profile, it is important to fully understand radiosonde data quality during winter storms. Over the years numerous factors have been noted to impact radiosonde data quality, including radiosonde icing (e.g., Bluestein et al. 1988; Miloshevich et al. 2009). Bluestein et al. (1988) suggested that icing was a potential source of error but

Corresponding author: Sean Waugh, sean.waugh@noaa.gov

DOI: 10.1175/JTECH-D-17-0074.1

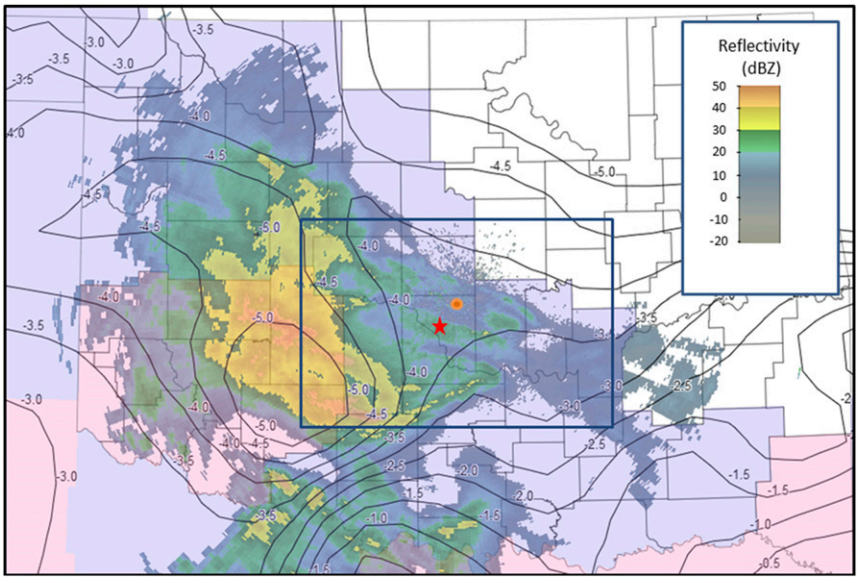

FIG. 1. Composite image showing KTLX WSR-88D radar reflectivity (dBZ) overlaid onto contours surface temperatures (°C) from the Oklahoma Mesonet and NWS-issued winter weather advisories (counties shaded in light blue) and winter storm warnings (counties shaded in pink) at 1400 UTC 24 Nov 2013. The location of the KTLX radar is indicated by the orange circle while the location of the two radiosonde launches (22.2 km at 220.8° azimuth from KTLX) is indicated by the red star. Areal coverage of the mPING precipitation type reports over central Oklahoma shown in Fig. 2 (dark blue box). Image generated using Oklahoma Mesonet Weatherscope software.

had no way of verifying it. Miloshevich et al. (2009) looked more specifically at icing but only in regard to the relative humidity (RH) sensor, which is heated and thus likely not to ice over during icing conditions. As noted by Cortinas et al. (2004), ice pellets falling to the surface in winter storms are often an indication of rain or drizzle aloft that can freeze upon impact with aircraft, potentially leading to severe ice accumulation (e.g., Bernstein et al. 1997; Zerr 1997; Politovich and Bernstein 2002; Bernstein et al. 2007). Surprisingly, however, the potential impact of these layers of freezing precipitation on radiosonde temperature measurements in winter storm systems has not been substantially addressed in the literature. For this reason, data from any radiosonde flown into these types of conditions should be examined with caution, as errors in the measured air temperature caused by icing of the radiosonde can be crucial for assessing precipitation type during forecasting efforts.

In this paper we present radiosonde data collected in a winter storm in Norman, Oklahoma, on 24 November 2013 and document the response of the temperature measurement to icing resulting from the radiosonde passing through freezing precipitation aloft. Section 2 provides an overview of the event and a description of the balloonborne Particle Size, Image, and Velocity (PASIV) microphysics instrument that was flown into the winter storm shortly after ice pellets were first reported at the surface. In section 3 we present and discuss radiosonde observations from the 1200 UTC Norman NWS (OUN) radiosonde flight and the research flight that carried the PASIV instrument. In particular, temperature data from the research flight appear to be compromised by icing. In section 4 data from the PASIV probe and nearby polarimetric KTLX (Oklahoma City, Oklahoma) WSR-88D radar are used to demonstrate that an elevated warm layer was not only present (though not observed in the project sounding profile) but was also likely warmer and possibly deeper than indicated by the radiosonde measurements. Section 5 presents a discussion that examines the conditions likely for radiosonde icing to occur, the implications of radiosonde icing on winter storm forecast operations, and the possible impact of radiosonde icing on model initialization during winter storm events. Section 6 summarizes the results.

2. Case overview

In the early morning hours of 24 November 2013, a band of winter precipitation approaching central Oklahoma from the southwest motivated the NWS to issue a winter weather advisory for much of northwest,

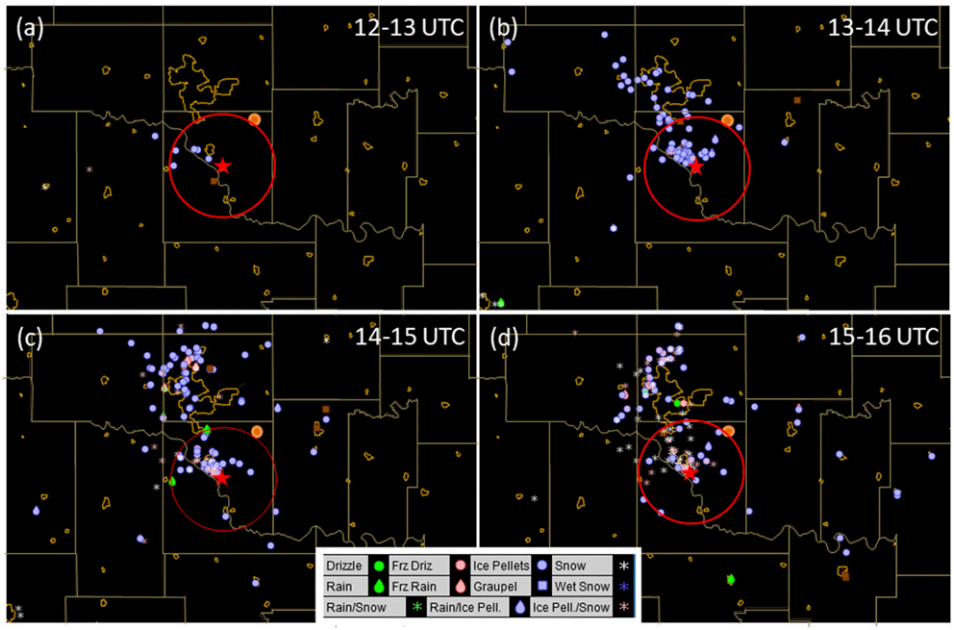

FIG. 2. mPING surface precipitation type reports over central Oklahoma (region corresponding to the box shown in Fig. 1) for (a) 1200–1300, (b) 1300–1400, (c) 1400–1500, and (d) 1500–1600 UTC 24 Nov 2013. The first mPING report of ice pellets in central Oklahoma occurred at 1243 UTC. As in Fig. 1, the location of the KTLX radar in each panel is indicated by the orange circle while the location of the two radiosonde launches (22.2 km at 220.8° azimuth from KTLX) is indicated by the red star. The red circle in each panel shows the 20-km range from the radiosonde launch location.

central, and south-central Oklahoma, and a winter storm warning for southwest Oklahoma, where up to 8 in. of snow accumulation was forecast. Figure 1 shows a radar image from the polarimetric KTLX WSR-88D radar image overlaid onto contours of Oklahoma Mesonet surface temperature and NWS winter weather advisories and winter storm warnings that were in effect at 1400 UTC, approximately 1 h after precipitation began in the Oklahoma City metropolitan area. Throughout the event, a mixture of rain, ice pellets, and snow fell across much of the OUN forecast area. Figure 2 shows surface observations of precipitation type reported to the Meteorological Phenomena Identification near the Ground (mPING) project (Elmore et al. 2014) over central Oklahoma from 1200 to 1600 UTC. Nearly an inch of ice pellets accumulated in the Norman area over the course of several hours (S. Waugh and T. J. Schuur, personal observation) before transitioning to snow.

At the National Weather Center (NWC), located on the University of Oklahoma's campus in Norman, a winter ballooning project was underway. The project aimed to launch a balloonborne videosonde known as the PASIV probe (Waugh et al. 2015) into winter precipitation events to collect in situ data on particle types that would allow for an investigation of the origins of the polarimetric "refreezing signature" associated with ice pellet events (Kumjian et al. 2013). The PASIV probe is capable of measuring the size, shape, and composition of individual particles, and the velocity of binned particles (Waugh et al. 2015). The instrument itself is composed of a Parsivel disdrometer (Löffler-Mang and Blahak 2001) and a high-definition video camera that allows detailed microphysics measurements to be made. The Parsivel disdrometer was heavily modified to reduce its size and weight in order to be flown on a balloonborne instrument. In addition to the PASIV probe, a Vaisala RS92-SGP radiosonde was flown to provide vertical profiles of temperature, pressure, humidity, winds, and GPS location information. Combining the two datasets, vertical profiles of particle size distributions and composition are possible with reference to the thermodynamic profile. This is particularly useful for determining where different particle types exist within the storm environment. A GoPro video camera was also attached to the instrument line at a location below the balloon and above the PASIV probe and radiosonde in order to video the launch from the balloon's perspective from above. It also served to document the conditions on the outside of the instruments. After the balloon launch, the instruments were recovered upon landing and the data collected, processed, and archived. Details of the data processing are described in Waugh et al. (2015).

3. Sounding observations

We here present and compare radiosonde data from the 1200 UTC OUN sounding (launched at 1100 UTC) and the project sounding (launched approximately 3 h later at 1400 UTC). The 1200 UTC 24 November 2013 OUN sounding that was launched from the NWC in Norman is shown in Fig. 3. At the time of this launch, mPING observations did not indicate the presence of any surface precipitation in central Oklahoma. The sounding shows subfreezing temperatures from the surface up to approximately 840 hPa, where a single shallow warm layer existed. The maximum temperature in this shallow warm layer was 0.6°C at 833 hPa. Above the warm layer, the temperature decreased by approximately 5°C before rebounding to −2.4°C. Above 600 hPa, the sounding cooled along a moist adiabat. The cloud base was encountered at approximately 700 hPa and conditions were nearly saturated from there up to the tropopause at 180 hPa. Below the cloud base, the environment was unsaturated. Of particular interest in the sounding is the shallow warm layer located between approximately 800 and 845 hPa, and the subfreezing temperatures that extended from below that layer to the surface. The 1155 UTC NWS area forecast discussion called for snow to begin falling in the Norman area within the next few hours.

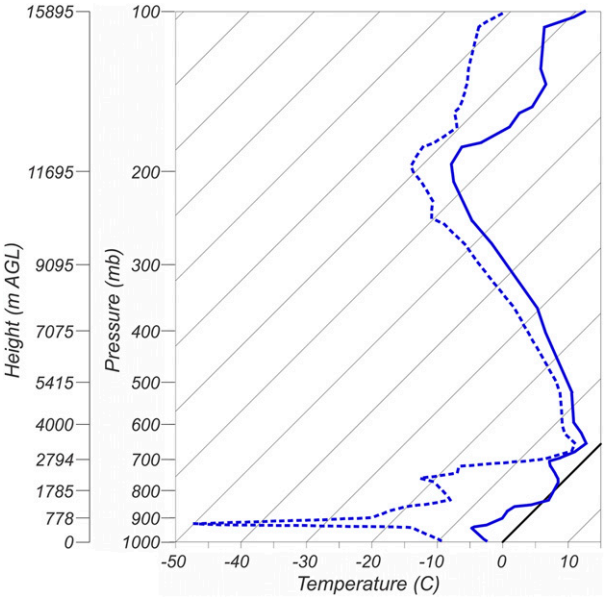

FIG. 3. 1200 UTC OUN sounding from Norman on 24 Nov 2013 with pressure (mb) and height (m AGL) coordinates. Sounding denotes near-freezing layer between 850 and 775 hPa with ~1°C warm nose near 840 hPa.

At roughly 1300 UTC, as ice pellets began to fall in Norman, the winter ballooning project began operations. Ice pellets continued to fall in Norman for several hours following the launch, with mPING reports indicating mostly snow falling about 20 km north of Norman with a mixture of ice pellets and freezing rain to the south (see Fig. 2). The winter ballooning project sounding, consisting of the radiosonde, PASIV instrument, and GoPro camera, was launched at 1401 UTC at the same location as the 1200 UTC OUN sounding and rose through actively falling precipitation. The project sounding is shown in Fig. 4. Though the raw project sounding data were recorded with a time resolution of 1 s, thereby providing a much higher temporal and vertical resolution than is typically available in real time to operational forecasters, we first present the project sounding data using the same number of levels, including the same significant levels, which were available on the operational sounding. Launched approximately 3 h after the 1200 UTC OUN sounding, the project sounding showed that the near-surface subfreezing layer had moistened and there was now a double warm nose present, the deepest of which spanned roughly from 715 to 765 hPa and appeared to be "isothermal" with a temperature of approximately 0°C. The lower, smaller warm nose located at approximately 850 hPa, which had a maximum temperature of 0.6°C in the earlier sounding, had cooled considerably and was entirely below 0°C by 1400 UTC. Above the isothermal layer, the temperature decreased steadily to a minimum temperature of −72°C at 100 hPa.

A more detailed comparison of the two soundings for the lowest 4000 m of the atmosphere, which approximately corresponds to 995 through 625 hPa in Figs. 3 and 4, is presented in Fig. 5, in which the project sounding is plotted using the raw 1-s data. Since the project sounding data presented in Fig. 5 have a better temporal and vertical resolution, they better illustrate the behavior of the project sounding temperature and dewpoint profiles through the isothermal layer. As with the previous figures, Fig. 5 indicates that the atmosphere exhibited a slight cooling of the warm layer between approximately 1.1 and 1.4 km AGL and significant warming above 2.0 km in the 3 h between the radiosonde launches. Unlike the earlier NWS sounding, the project sounding temperature profile also exhibits a sharp unrealistic discontinuity at the 0°C level and then fluctuates between ±0.5°C within a layer from roughly 2 km to ~550 m above. The dewpoint data were flagged as missing over approximately this same interval from the freezing level to 550 m above the freezing level. Missing data points are typically not plotted or available to forecasters in operational soundings, nor were they plotted in Fig. 4. As will be discussed in more detail in section 5, these missing dewpoints are likely attributable

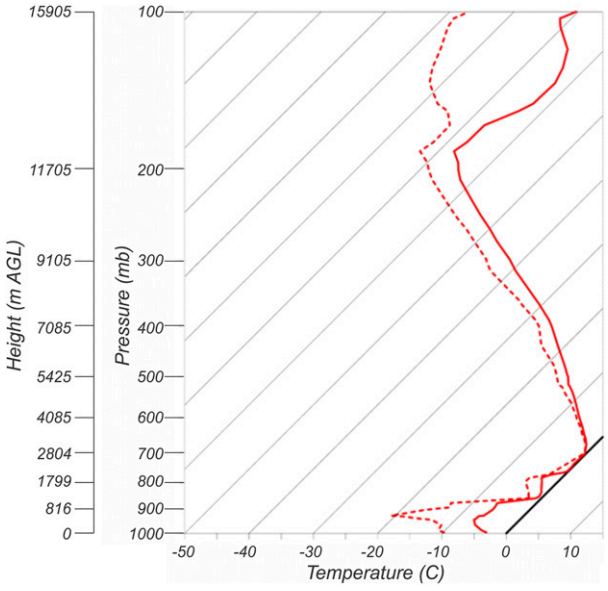

FIG. 4. 1400 UTC sounding taken during the winter ballooning project with pressure (mb) and height (m AGL) coordinates. The isothermal layer at 0°C between 775 and 680 hPa is shown. Compared to the 1200 UTC sounding, the RH has increased substantially in the near-surface layer.

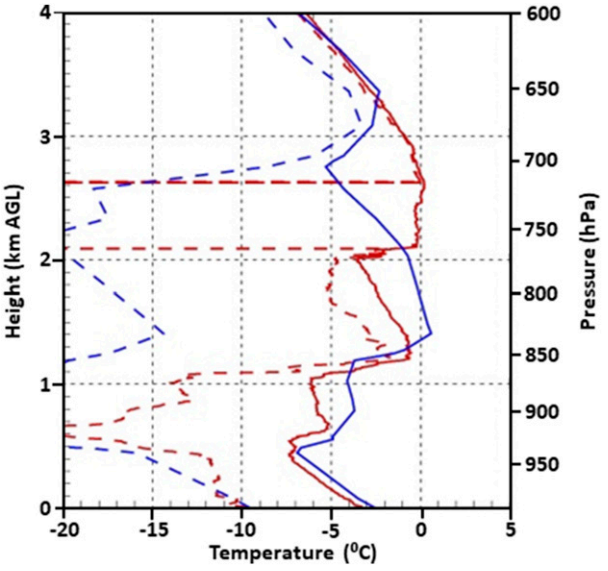

FIG. 5. Detailed comparison of the OUN sounding (launched at 1100 UTC; blue lines) and instrumented project sounding (launched at 1400 UTC; red lines). Temperature profiles (solid lines) and dewpoints (dashed lines) are shown for each sounding. Right scale shows corresponding pressure levels from the project sounding. Pressure at 0 km AGL was 996 hPa.

to RH measurements exceeding 100%, as a result of artificially low temperature measurements caused by icing, resulting in computed dewpoints that exceeded the measured temperatures.

Before we further evaluate the cause of the ~550-m-deep layer that exhibited temperatures that fluctuated between ±0.5°C in Fig. 5, it should be noted that isothermal layers with a temperature near 0°C have been documented and described by numerous previous studies (e.g., Stewart 1984; Heymsfield et al. 2015). That is, when frozen precipitation falls into an elevated warm layer, it melts and cools the environment around it by absorbing latent heat, often leading to a quasi-0°C layer. This process continues as long as the temperature is above freezing and frozen precipitation continues to fall into the layer. Examining the temperature profile, one would see an isothermal layer at 0°C at the top of the temperature inversion in the ML, which would work its way down toward the surface in time. The effect would be to slowly erode the warm layer, transitioning the falling precipitation to snow at the surface as melting ceased and a warm nose was no longer present.

In our case a careful examination of the temperature profile in Fig. 5 (also Fig. 10a, which provides an even more detailed view) shows that while the *maximum* temperature in our project sounding was 0.2°C, that maximum was merely the peak temperature within a very shallow layer of only ~200 m (2.45–2.65 km) in depth that had temperatures > 0°C. While that layer may have been of sufficient strength to melt the smallest of ice particles that fell into the layer, we do not believe that it was of sufficient strength to account for the melting of the larger ice particles that, after subsequent refreezing, would be responsible for the larger ice pellets that were observed at the time of the balloon launch.

An additional argument against the isothermal layer in our project sounding being due to melting is that the bulk of the temperatures in the ~350-m-deep (2.1–2.45 km) isothermal layer that lies below the shallow ~200-m-deep warm layer were slightly *less than* 0°C. Over time, melting of ice particles falling into a warm layer from above would cause the temperature to trend toward 0°C. It could not, however, account for a deep layer of temperatures *less than* 0°C. Indeed, this observation is more consistent with thermal damping. That is, as the iced radiosonde ascended into an elevated warm layer, the ice coating on the radiosonde would initially damp the temperature response, resulting in temperatures that were at or slightly below 0°C. As the ice on the radiosonde sensor slowly melted, the temperature would be expected to slowly recover to temperatures > 0°C. This is what is seen in our temperature profile.

In the next section, we present additional evidence that icing of the radiosonde likely led to an erroneous isothermal layer, rather than to a more pronounced warm layer, in the project sounding temperature profile.

4. PASIV probe and polarimetric radar observations

While the project sounding does not indicate a well-defined ML, we present evidence from independent PASIV probe and polarimetric radar data sources to demonstrate that an elevated warm layer was not only present, but likely warmer than indicated by the project radiosonde temperature data.

a. PASIV observations

Particle sizes and counts from the disdrometer observations are shown in Fig. 6. The data show a dramatic increase in average and maximum particle sizes from approximately 2200 to 3100 m (780–700 hPa), a layer that encompasses the isothermal layer indicated by the project sounding. This increase in particle sizes is consistent with what would be expected for an ML as particles melt and stick together, broadening the size distribution to larger particle sizes (Willis and Heymsfield 1989; Heymsfield et al. 2015).

Images from the PASIV high-definition video camera within this layer can also aid directly in particle identification and the presence of liquid water. With this instrument object classification is based on visual aspects alone and makes no attempt to describe the specific crystal type or aspects such as the degree of riming present (Waugh 2016). Regular ice crystals are typically less than 2 mm in diameter and have highly elliptical, symmetric, smooth shapes (Waugh 2016). Irregular crystals are ice crystals with largely nonspherical shapes often containing protrusions. Crystals and aggregates from Heymsfield and Musil (1982) and aggregates of assemblages from Pruppacher and Klett (1997) would fall into this category. Within the imager, liquid water and ice have very different reflective properties that make them distinguishable. Liquid water is identifiable from frozen particles as a result of the semitransparent structure and dual-lens reflections caused by the reflectivity of the water surface. The light-emitting diode (LED) panels show up as separate lenses closely spaced, with a barely visible outline of the transparent structure between. Conversely, ice particles tend to scatter light evenly, producing bright milky white objects with a definable edge.

Given this behavior, Fig. 7 indicates a mixture of particle types, including irregular crystals, regular small ice crystals, and liquid water drops. Figure 7a shows an example image of observed regular and irregular crystals, while Fig. 7b shows several small ice crystals and a liquid water droplet. Both images were taken in the isothermal layer near 737 hPa and a temperature of −0.3°C. The red arrow in Fig. 7b denotes the location of a liquid water droplet. The PASIV instrument therefore indicates the presence of liquid water in this layer, suggesting the presence of an ML.

b. Polarimetric KTLX WSR-88D observations

Evidence of an elevated warm layer is also provided by the polarimetric KTLX WSR-88D radar, located 22.2 km to the northeast of the sounding launch site. In addition to radar reflectivity Z, polarimetric radars collect several variables, including differential reflectivity Z_{DR}, correlation coefficient ρ_{HV}, and differential phase Φ_{DP}, which have been shown to provide valuable information that can be used to detect the presence of an ML (e.g., Brandes and Ikeda 2004; Giangrande et al. 2008). Specifically, the polarimetric signature of an ML is characterized by a pronounced maxima in Z and Z_{DR} and a minima in ρ_{HV}. During the entire event, the KTLX radar collected data in volume coverage pattern (VCP) 31, which has a maximum elevation of 4.5°.

Figure 8 shows the KTLX radar variables Z, Z_{DR}, and ρ_{HV} from the 4.5° elevation scan at 1409 UTC—the time that the project radiosonde was passing through the isothermal layer between approximately 780 and 700 hPa. The black rings on each panel show the ranges where the 4.5° elevation scan intersects the 1.50-, 1.75-, 2.00-, 2.25-, and 2.50-km heights, while the white dot indicates the balloon launch site. As noted by Giangrande et al. (2008), the well-pronounced maxima in Z and Z_{DR} and minima in ρ_{HV} found in MLs are typically not found at the same altitude, with the maximum in Z commonly observed at a higher altitude and a more distant slant range than both the maximum in Z_{DR} and the minimum in ρ_{HV}. The polarimetric measurements of enhanced Z and Z_{DR} and reduced ρ_{HV} show the clear presence of an ML over central Oklahoma, with an ML height of ~2 km over the launch site and good agreement with the height of both the isothermal layer in the project sounding (Figs. 4 and 5) and the maxima in particle sizes indicated by the PASIV disdrometer data (Fig. 6).

A quasi-vertical profile (QVP; Ryzhkov et al. 2016) of the polarimetric data is also presented to document the temporal evolution of the ML signature for the event as it passed over central Oklahoma (Fig. 9). QVPs are generated by azimuthally averaging polarimetric variables from a series of radar volumes to generate time–height plots that show the temporal evolution of polarimetric signatures and microphysical processes (e.g., Kumjian et al. 2013; Ryzhkov et al. 2016; Van den Broeke et al. 2016; Kumjian and Lombardo 2017). Since QVPs are generated by azimuthal averaging, it is necessary to assume some degree of horizontal continuity, with the radius over which the averaging takes place increasing with height. Because of this, QVPs are generally produced using radar data from higher elevation angles. Since KTLX radar data on 24 November 2013

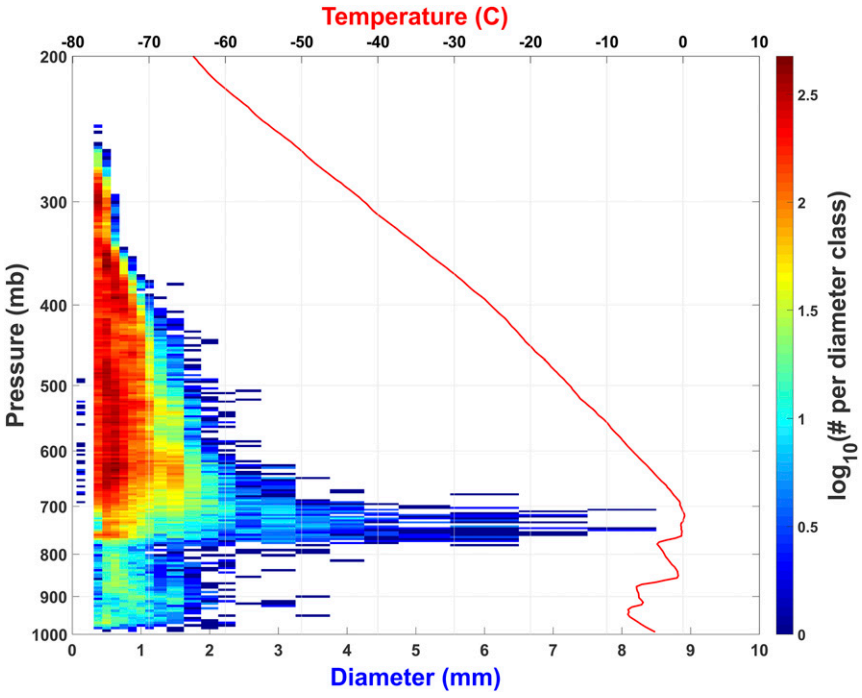

FIG. 6. Particle sizes and counts from the modified Parsivel size imaging probe that was flown on the project balloon sounding. Number of particles per size bin is shown on a logarithmic scale as indicated by the color bar. Temperature profile (red line) from the project sounding (Fig. 4) is shown for comparison.

were collected using VCP 31, we are limited to producing QVPs at the maximum elevation of 4.5° for this event. While this may be a limitation for examining the evolution of microphysical features at higher levels in the cloud, the primary interest of this analysis is the evolution of the ML signature, located below 3 km in height (corresponding to a averaging radius of <40 km for 4.5° elevation) during the 24 November 2013 event. We therefore believe the 4.5° elevation QVP is justified to illustrate this evolution.

As can be seen in the Z and ρ_{HV} fields in Fig. 9, a clear, albeit initially weak, brightband signature is evident starting at approximately 1300 UTC, approximately 1 h before the launch of the project flight. With time, this signature is seen to slowly intensify and descend. Between approximately 1600 and 1800 UTC, the bright band, as indicated by the high Z, high Z_{DR}, and low ρ_{HV}, suddenly descends to ground level, likely in association with evaporative cooling of sufficient strength to cool the entire column below the bright band and allow wet snow to reach the surface (Kumjian et al. 2016). This transition occurred as the surface cold pool that was over southwestern Oklahoma at 1400 UTC (see mesonet surface temperature observations in Fig. 1) passed over central Oklahoma and was also in agreement with mPING observations, which showed an increase in snow reports over central Oklahoma during this period (1600–1800 UTC).

The presence of a polarimetric brightband signature is further highlighted by Fig. 10, which shows a comparison of the project sounding's temperature, and Z, Z_{DR}, and ρ_{HV} QVP profiles between 1.5 and 3.5 km at 1400 UTC. The profiles of the polarimetric variables in the figure are consistent with what is typically observed in the ML, that is, enhanced Z and Z_{DR} and reduced ρ_{HV}, with the maximum in Z located at a higher altitude than both the maximum in Z_{DR} and minimum in ρ_{HV} (Giangrande et al. 2008), collocated in height with the expected location of the ML.

5. Discussion

While freezing precipitation has been noted to form from warm rain processes (Huffman and Norman 1988; Rauber et al. 2000), surface reports of ice pellets at the surface often provide strong evidence of freezing rain aloft formed by the classical melting mechanism (Hanesiak and Stewart 1995). In such cases the existence of ice pellets at the surface provides evidence of a warm layer aloft. In this case both the PASIV probe and

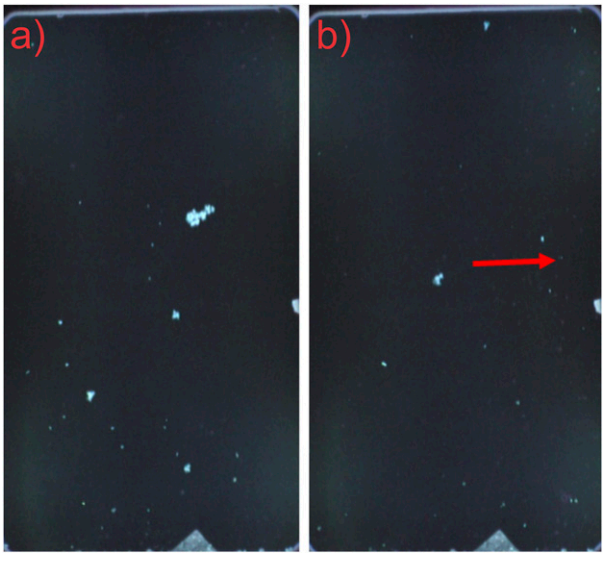

FIG. 7. Images from the PASIV probe in the "isothermal layer" at an altitude of 2730 m (737 hPa, −0.3°C) showing ice crystals: (a) aggregates and (b) a liquid water drop (indicated by the red arrow).

polarimetric KTLX WSR-88D data provide additional evidence of an elevated warm layer. As the presence of an ML is suggested by the PASIV probe and the radar, an examination of why the project sounding did not also detect it is warranted.

The layer between 850 and 775 hPa, below the ML, was characterized by subfreezing temperatures down to −3°C with nearly saturated conditions with respect to water, supersaturated conditions with respect to ice, and the presence of water droplets as indicated by the PASIV probe. Given all of these conditions, riming was an active process in this environment and the supercooled droplets present would freeze on contact with any surface. If ice was present on the radiosonde in the ML, it would melt at 0°C until the phase change was complete and the ice had melted. As this process continued, the radiosonde would measure the temperature of the ice and any water present on the sensing element, not the ambient air temperature. Temperatures of 0°C would continue to be reported as long as the melting ice remained on the sensing element, despite the ambient environmental temperature being above freezing.

It is suggested that the sequence of events leading to icing of the radiosonde in the refreezing layer prevented measurements of the ambient air temperature and was responsible for the 0°C isothermal layer reported by the radiosonde where the ML was located according to radar and PASIV probe observations (~2–2.5 km AGL). The slowly melting ice covering the radiosonde likely kept the reported temperature near 0°C, though the actual temperature was likely warmer than 0°C by at

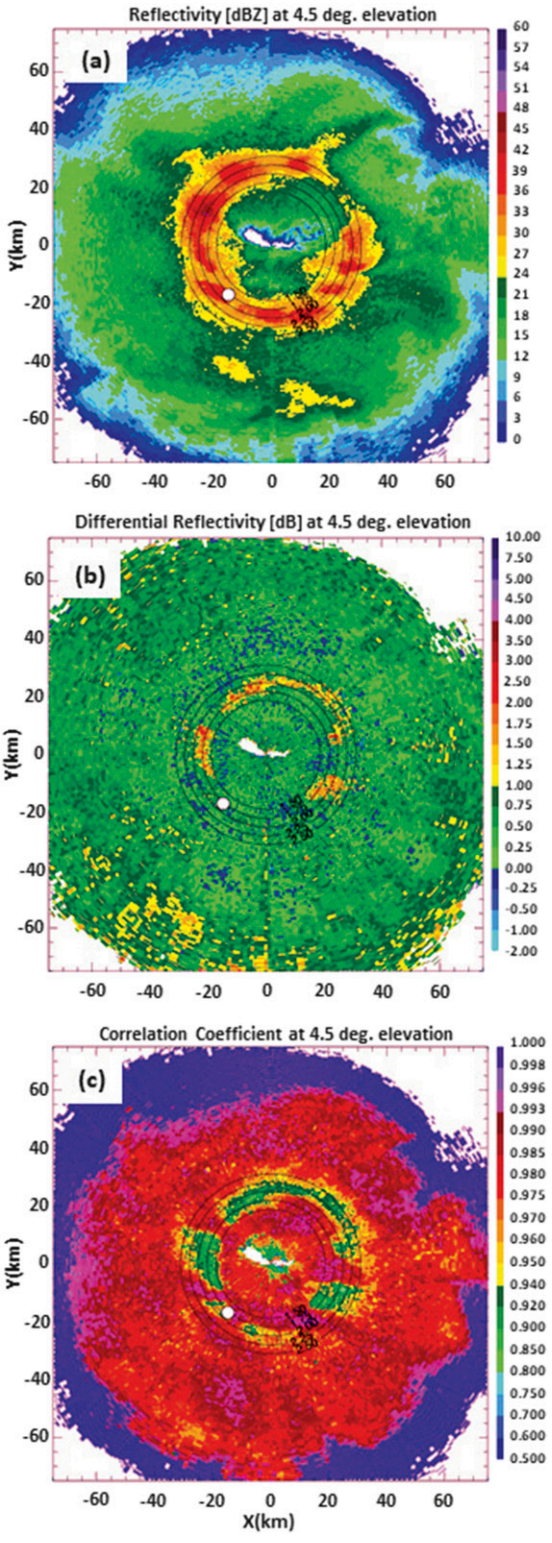

FIG. 8. Polarimetric KTLX WSR-88D 4.5° (a) Z, (b) Z_{DR}, and (c) ρ_{HV} at 1409 UTC. Location of the radiosonde launch (22.2 km at 220.8° azimuth from KTLX; white dot) is indicated. Range rings show 1.50-, 1.75-, 2.00-, 2.25-, and 2.50-km heights of the 4.5° elevation beam, indicating the height of the melting layer/bright band (high Z and Z_{DR}, low ρ_{HV}) over central Oklahoma.

least a few degrees. Because of the roughly 0.5-km-deep ML, and the amount of ice built up on the radiosonde, complete melting of ice on the radiosonde was not achieved. Therefore, the temperature in the warm layer, as sensed by the radiosonde, never rose significantly above 0°C. As the radiosonde continued to ascend above the ML and the environmental temperature decreased, melting of the ice layer on the radiosonde ceased. Any ice that remained on the radiosonde's sensing elements at this point acted as a thermal insulator for the remainder of the flight, as the radiosonde measured the temperature of the ice coating. Any environmental changes in the air temperature would have to change the ice temperature before being sensed by the radiosonde. This effectively acted to slow the response of the temperature sensor, thereby causing the radiosonde to consistently overestimate the temperature at levels above the ML.

Figure 11 shows two images captured from the GoPro camera, one shortly after launch (Fig. 11a) and another once the instrument train exited the top of the cloud layer and rose into sunlight, in which it possible to see a clear layer of ice buildup on the normally smooth, flat white radiosonde casing and the highly reflective temperature sensing element (Fig. 11b, indicated by a red arrow). The Fig. 11a image was taken at 562 m (968 hPa, −5.7°C, 65% RH), while Fig. 11b image was taken at roughly 9920 m (279 hPa, −46°C, 68% RH). The sensing element is roughly 0.2 mm thick and is normally very difficult to see, particularly from a wide-angle camera lens such as the GoPro and at the distance the camera was located from the radiosonde. In Fig. 11b, however, the upper portion of the sensing element (portion that is closest to the red arrow) shows a clear increase in thickness toward the top of the radiosonde arm, indicating the likely presence of ice on the temperature wire. This figure confirms that ice was present on the radiosonde and was likely responsible for the lack of an observed ML. The RS92-SGP radiosonde has a hydrophobic coating applied to the temperature sensor (Vaisala 2010) in an effort to reduce liquid water for the purposes of evaporative cooling, but no mention is made of any protection against ice buildup. Regardless, the coating did not stop the buildup of ice on the temperature sensing element. The highly reflective sensor arm makes it difficult to determine whether ice is present on the remaining sensing elements. However, the RS92-SGP utilizes dual RH sensors, alternating between observations on each one as the other is heated to remove any contaminants. Given this instrument design, it is unlikely that the RH sensors maintained any lingering ice coverage.

Given the observed icing of the radiosonde, the missing dewpoint values in the project sounding (Fig. 5) deserve a special note. In Fig. 5 the region corresponding to the isothermal layer on the project sounding was characterized by dewpoints that were flagged as missing. This may lead to the conclusion that the dewpoint data themselves are bad and not to be trusted. Examining the raw 1-s data obtained from the project sounding, the RH values in this layer are over 100%, thereby resulting in dewpoints that are higher than the observed temperature, which is being artificially lowered as a result of the icing. The automatic processing of the Vaisala system flags these values as unphysical and removes the dewpoints but leaves the temperature data as a result of its inability to recognize that both are likely incorrect. As discussed by the NWS manual *Rawinsonde Observations* (Caldwell 2010), RH readings can be biased too high when the sensor is coated by water or ice; however, it makes no mention of icing for temperature readings. Without examination of the raw data and knowledge of radiosonde icing, one may still assume that the temperature data are correct, which could lead to complications in forecast scenarios.

It is unclear how often conditions necessary for radiosonde icing are present in winter storms. However, it is important to note that one of the radiosondes typically used by the NWS (Vaisala RS92-SGP) is the same type that was used for the project flight presented in this study. We therefore do not believe this was an isolated event. As with aircraft icing, it is likely that radiosonde icing is favored in particular winter storm environments. Numerous studies have found relationships between the depth and intensity of the elevated warm and lower cold layers and the presence of either ice pellets or freezing rain at the surface (Czys et al. 1996; Rauber et al. 2000; Bourgouin 2000; Reeves et al. 2014). Freezing rain is more commonly produced by environments with MLs that are warmer and/or deeper than those that produce ice pellets. That is, if incomplete melting of ice particles takes place in an ML, drops that still contain ice cores are present, which can easily refreeze to form ice pellets when they enter the cold layer below. On the other hand, if complete melting of ice particles takes place in an ML, subsequent refreezing to form ice pellets requires an ice nucleation process (Pruppacher and Klett 1997; Kumjian et al. 2013; Reeves et al. 2016). Insight might also be gained by examining conditions that produce significant icing of aircraft or other manufactured structures. For example, several studies have examined environmental conditions associated with aircraft icing (e.g., Sand et al. 1984; Politovich 1989; Ashenden and Marwitz 1998). In particular, environmental layers

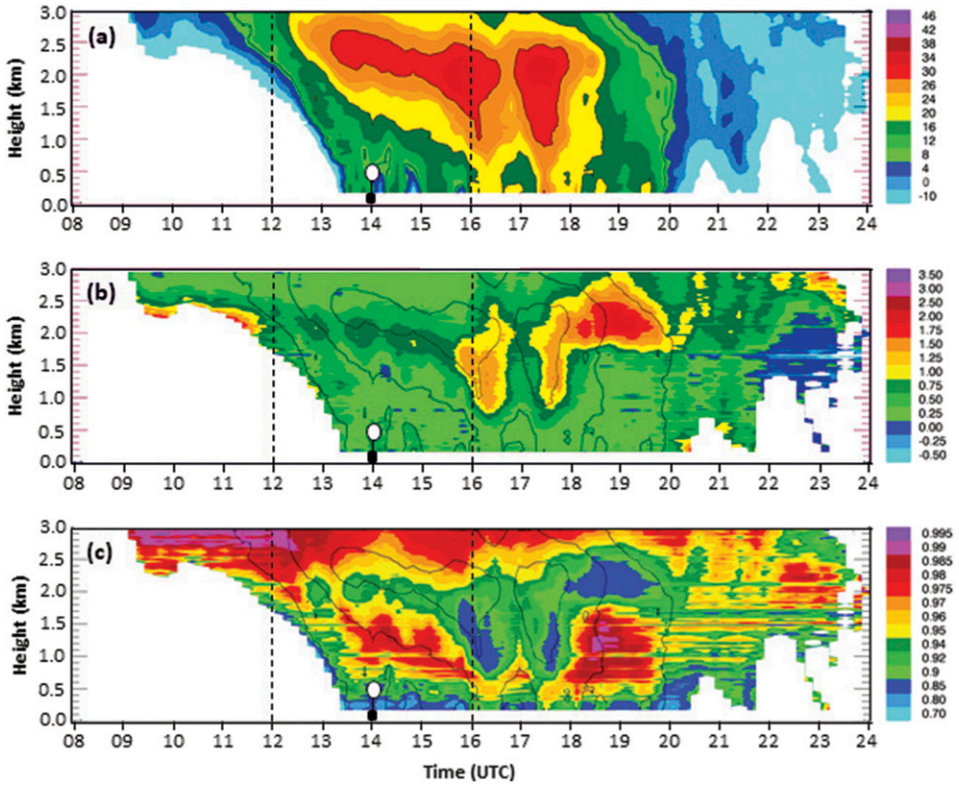

FIG. 9. QVPs of 4.5° elevation polarimetric KTLX WSR-88D (a) Z, (b) Z_{DR}, and (c) ρ_{HV} showing the evolution of the ML/brightband intensity and height as the winter storm passed over central Oklahoma. Reflectivity contours in (b) and (c) of 10, 20, and 30 dBZ (overlaid contours). Vertical dashed lines indicate time intervals corresponding to mPING observations depicted in Fig. 2 balloon at 14 UTC indicates the time at which the project sounding was launched.

containing an abundance of supercooled large drops (SLD) with diameters $> 50\,\mu$m have frequently been mentioned as favorable for aircraft icing. Cober et al. (2001) examined the icing environments encountered in 38 research aircraft flights, including 12 in which SLD were found to have formed in an environment very similar to that presented here, that is, where ice crystals were found to have melted in an elevated warm layer and cooled as they fell into a lower cold layer. Insight might also be gained from studies that have examined favorable icing conditions of other man-made structures. Banitalebi Dehkordi et al. (2013), for example, studied the effect of drop size distributions and liquid water content on the rate of ice accretion on electrical tower legs.

While in situ observations, including pictures from the GoPro camera, provide clear evidence of an ice coating on the radiosonde, a determination of whether the ice coating is from collection/refreezing of partially melted ice particles or the riming of small drops is not possible without closer inspection of the radiosonde. From the results of past studies, we suspect that radiosonde icing is likely favored in subfreezing layers where liquid water is present. In this case the icing likely takes place in the subfreezing layer beneath the ML where incomplete melting of ice particles has taken place. As has been shown to be the case for aircraft icing, we speculate that radiosonde icing might also exhibit a dependence on supercooled drop size.

In addition to forecast implications, undiagnosed temperature measurement errors associated with radiosonde icing have the potential to adversely impact other areas of research that rely heavily on sounding data collected in these types of conditions. For example, numerous studies in the past have used large databases of winter storm soundings to develop winter precipitation type climatologies or empirical techniques to determine precipitation type at the surface. While it is not suggested that previous studies used data that were corrupted or that their conclusions were incorrect, the data presented here suggests that studies that do use radiosonde data collected in winter storm conditions that are favorable for icing could benefit from additional examination.

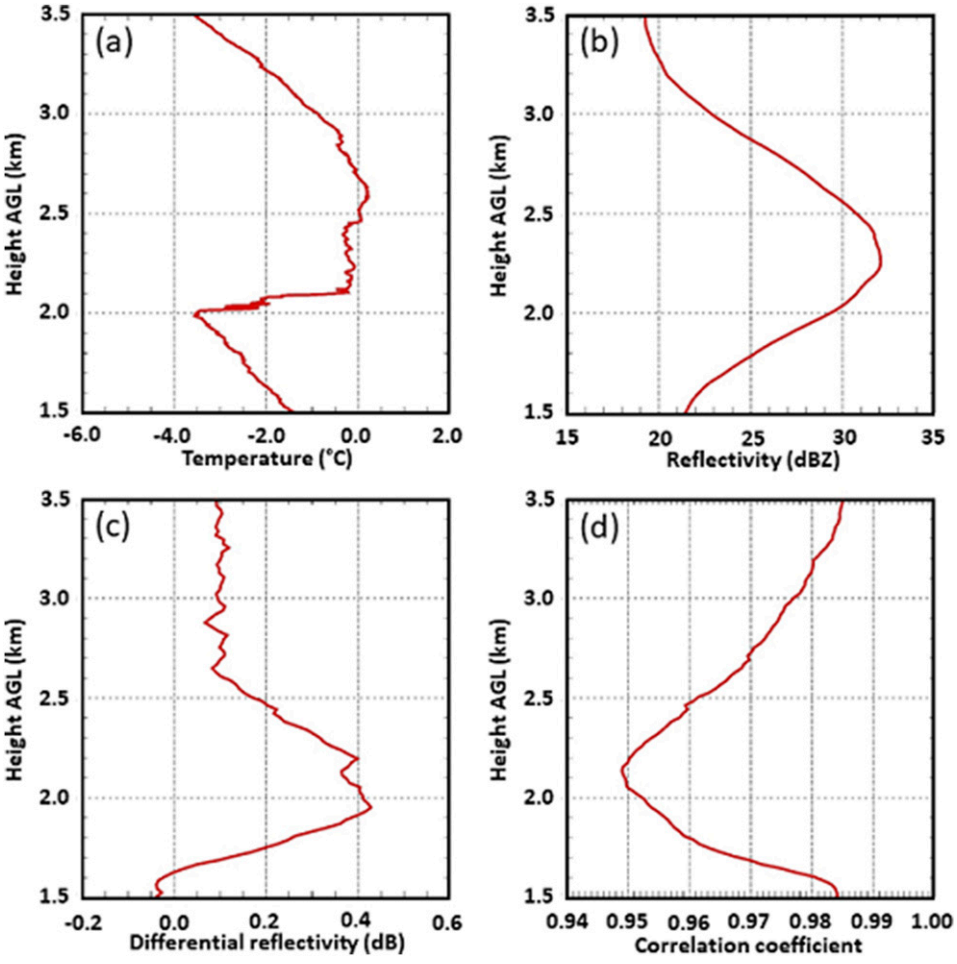

FIG. 10. Comparison of the project sounding's (a) temperature, (b) QVP profile of Z, (c) QVP profile of Z_{DR}, and (d) QVP profile of ρ_{HV} between 1.5 and 3.5 km (centered on the expected location of the ML) at 1400 UTC.

6. Conclusions

Evidence of significant radiosonde icing in a winter weather event that produced ice pellets at the surface is presented. While the radiosonde itself did not indicate the presence of a significant elevated warm layer, supplemental data provided by both the balloonborne PASIV disdrometer and polarimetric KTLX WSR-88D radar indicate that an elevated warm layer did indeed exist. Icing conditions, whether by riming or depositional growth, caused the buildup of ice on the temperature sensing element of the radiosonde which led to the misrepresentation of the true environment. An isothermal layer was observed in the sounding that was caused by the melting of ice present on the radiosonde, masking the ambient environmental temperature and complicating the forecast decision-making process utilizing those data by misrepresenting the environment. The presence of this ice was observed through a GoPro camera that was situated above the radiosonde.

With consideration of the potential errors in temperature caused by radiosonde icing present in winter weather soundings, relying on soundings taken in winter events must be approached with extreme caution. Even small measurement errors in the temperature profile of winter storms can have a dramatic impact on the precipitation type forecast for the surface. For example, several studies have demonstrated that discrimination between freezing rain and ice pellets is largely determined by both the depth and intensity of the elevated warm ML and low-level cold refreezing layer. If the ML is of insufficient depth and intensity to result in the complete melting of ice particles that fall into it, then any resulting ice core that remains in a drop that exits the ML can serve as an ice nucleus below, thus providing an opportunity for radiosonde icing. Not only are these conditions favorable for radiosonde icing, but any resulting underestimation of the intensity of the ML might impact the forecast of precipitation type. We believe radiosonde icing is favored

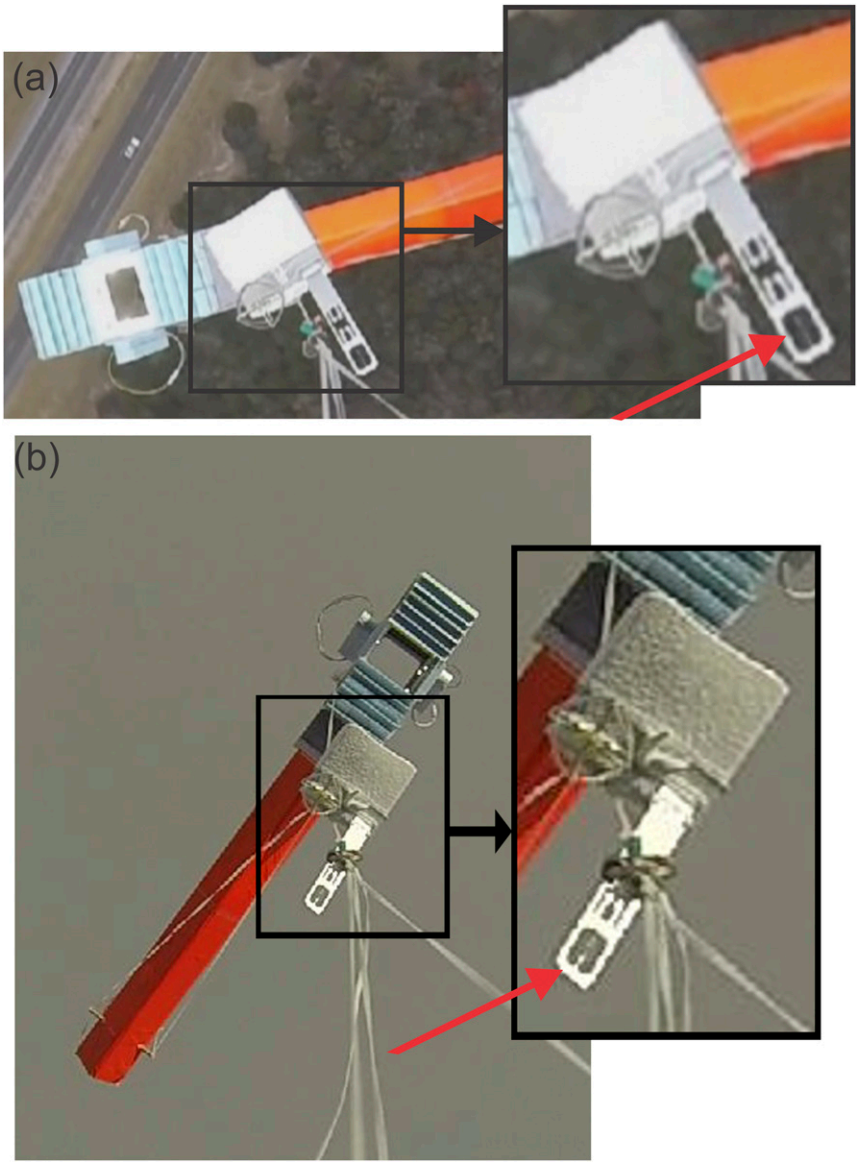

FIG. 11. GoPro image of instrument train at an altitude of (a) 562 m (968 hPa, −5.7 C, 65% RH) and (b) 9920 m (279 hPa, −46°C, 68% RH). GoPro camera is looking "down" at instruments. Ascending instruments just after launch, prior to ice buildup, are shown in (a). Instrument exiting the top of the cloud is shown in (b), in which the gray background is cloud top. Ice buildup on the white structure of the radiosonde and the temperature sensing element is noticeable. (inset) Expanded view of radiosonde in both cases. Position of the temperature sensing element is indicated (red arrow). Highly reflective sensor arm makes it difficult to discern the presence of ice on the RH sensor.

in refreezing conditions beneath elevated warm layers of low to moderate intensity.

Given that the daily soundings provided by the NWS are of fundamental importance to daily forecast and warning operations, it is crucial that the data are as accurate as possible. With the potential implications of poor winter storm radiosonde data quality on numerical model initialization, it is suggested that other methods of quantifying ML presence, strength, and height be supplemented where radiosonde data are questionable. Consistent monitoring of ML height and intensity using polarimetric QVPs, preferably at higher elevation angles than were available for this study, could be used as a supplement for sounding data when the radiosonde data cannot be trusted. These radar data would serve not only to initialize models in winter storm situations where

temperature data are questionable, but also to be assimilated into numerical models at higher temporal resolution than is possible with radiosonde observations for fast evolving winter storm situations.

Without careful examination of the sounding or data provided by other instrumentation, it is difficult to recognize radiosonde icing. Therefore, all available data, such as radiosonde, model, and radar, should be examined during decision-making to determine whether an ML is indeed present. For cases where isothermal layers such as the one presented here are observed by a radiosonde and an ML is found to exist through other instruments, those radiosonde data should be identified and excluded.

Acknowledgments. The authors thank Dr. Heather Reeves, Dr. Kim Elmore, and two anonymous reviewers for providing thorough reviews of this manuscript. Erica Griffin helped process the radar data and produce QVPs. This project would not have been possible without the assistance of several University of Oklahoma undergraduate and graduate students, who graciously volunteered their time to help with the launch of the weather balloon and the PASIV instrument. Funding for this work was by a National Severe Storms Laboratory Directors Discretionary Research Fund award and by the NOAA/Office of Oceanic and Atmospheric Research under NOAA–University of Oklahoma Cooperative Agreement NA11OAR4320072, U.S. Department of Commerce.

REFERENCES

Ashenden, R., and J. D. Marwitz, 1998: Characterizing the supercooled large drop environment with corresponding turboprop aircraft response. *J. Aircr.*, **35**, 912–920, https://doi.org/10.2514/2.2386.

Banitalebi Dehkordi, H., M. Farzaneh, P. Van Dyke, and L. E. Kollar, 2013: The effect of droplet size and liquid water content on ice accretion and aerodynamic coefficients of tower legs. *Atmos. Res.*, **132–133**, 362–374, https://doi.org/10.1016/j.atmosres.2013.07.002.

Bernstein, B. C., T. A. Omeron, F. McDonough, and M. K. Politovich, 1997: The relationship between aircraft icing and synoptic-scale weather conditions. *Wea. Forecasting*, **12**, 742–762, https://doi.org/10.1175/1520-0434(1997)012<0742:TRBAIA>2.0.CO;2.

——, C. A. Wolff, and F. McDonough, 2007: An inferred climatology of icing conditions aloft, including supercooled large drops. Part I: Canada and the continental United States. *J. Appl. Meteor. Climatol.*, **46**, 1857–1878, https://doi.org/10.1175/2007JAMC1607.1.

Bluestein, H. B., E. W. McCaul Jr., G. P. Byrd, and G. R. Woodall, 1988: Mobile sounding observations of a tornadic storm near the dryline: The Canadian, Texas storm of 7 May 1986. *Mon. Wea. Rev.*, **116**, 1790–1804, https://doi.org/10.1175/1520-0493(1988)116<1790:MSOOAT>2.0.CO;2.

Bosart, L. F., and J. W. Nielsen, 1993: Radiosonde penetration of an undilute cumulonimbus anvil. *Mon. Wea. Rev.*, **121**, 1688–1702, https://doi.org/10.1175/1520-0493(1993)121<1688:RPOAUC>2.0.CO;2.

Bourgouin, P., 2000: A method to determine precipitation types. *Wea. Forecasting*, **15**, 583–592, https://doi.org/10.1175/1520-0434(2000)015<0583:AMTDPT>2.0.CO;2.

Brandes, E. A., and K. Ikeda, 2004: Freezing-level estimation with polarimetric radar. *J. Appl. Meteor.*, **43**, 1541–1553, https://doi.org/10.1175/JAM2155.1.

Caldwell, D., 2010: Rawinsonde observations. Operations and Services, Upper Air Program NWSPD 10-14, National Weather Service Manual 10-1401, 208 pp., http://www.nws.noaa.gov/directives/sym/pd01014001curr.pdf.

Cober, S. G., G. A. Isaac, and J. Walter Strapp, 2001: Characterization of aircraft icing environments that include supercooled large drops. *J. Appl. Meteor.*, **40**, 1984–2002, https://doi.org/10.1175/1520-0450(2001)040<1984:COAIET>2.0.CO;2.

Cortinas, J. V., Jr., B. C. Bernstein, C. C. Robbins, and J. W. Strapp, 2004: An analysis of freezing rain, freezing drizzle, and ice pellets across the United States and Canada: 1976–90. *Wea. Forecasting*, **19**, 377–390, https://doi.org/10.1175/1520-0434(2004)019<0377:AAOFRF>2.0.CO;2.

Czys, R. R., R. W. Scott, K. C. Tang, R. W. Pryzbylinski, and M. E. Sabones, 1996: A physically based, nondimensional parameter for discriminating between locations of freezing rain and ice pellets. *Wea. Forecasting*, **11**, 591–598, https://doi.org/10.1175/1520-0434(1996)011<0591:APBNPF>2.0.CO;2.

Elmore, K. L., Z. L. Flamig, V. Lakshmanan, B. T. Kaney, V. Farmer, H. D. Reeves, and L. P. Rothfusz, 2014: mPING: Crowd-sourcing weather reports for research. *Bull. Amer. Meteor. Soc.*, **95**, 1335–1342, https://doi.org/10.1175/BAMS-D-13-00014.1.

Giangrande, S. E., J. M. Krause, and A. V. Ryzhkov, 2008: Automated designation of the melting layer with a polarimetric prototype of the WSR-88D radar. *J. Appl. Meteor. Climatol.*, **47**, 1354–1364, https://doi.org/10.1175/2007JAMC1634.1.

Hanesiak, J. M., and R. E. Stewart, 1995: The mesoscale and microscale structure of a severe ice pellet storm. *Mon. Wea. Rev.*, **123**, 3144–3162, https://doi.org/10.1175/1520-0493(1995)123<3144:TMAMSO>2.0.CO;2.

Heymsfield, A. J., and D. J. Musil, 1982: Case study of a hailstorm in Colorado. Part II: Particle growth processes at mid-levels deduced from *in-situ* measurements. *J. Atmos. Sci.*, **39**, 2847–2866, https://doi.org/10.1175/1520-0469(1982)039<2847:CSOAHI>2.0.CO;2.

——, A. Bansemer, M. R. Poellot, and N. Wood, 2015: Observations of ice microphysics through the melting layer. *J. Atmos. Sci.*, **72**, 2902–2928, https://doi.org/10.1175/JAS-D-14-0363.1.

Huffman, G. J., and G. A. Norman Jr., 1988: The supercooled warm rain process and the specification of freezing precipitation. *Mon. Wea. Rev.*, **116**, 2172–2182, https://doi.org/10.1175/1520-0493(1988)116<2172:TSWRPA>2.0.CO;2.

Kumjian, M. R., and K. A. Lombardo, 2017: Insights into the evolving microphysical and kinematic structure of the northeastern U.S. winter storms from dual-polarization Doppler radar. *Mon. Wea. Rev.*, **145**, 1033–1061, https://doi.org/10.1175/MWR-D-15-0451.1.

——, A. V. Ryzhkov, H. D. Reeves, and T. J. Schuur, 2013: A dual-polarization radar signature of hydrometeor refreezing in winter storms. *J. Appl. Meteor. Climatol.*, **52**, 2549–2566, https://doi.org/10.1175/JAMC-D-12-0311.1.

——, S. Mishra, S. E. Giangrande, T. Toto, A. V. Ryzhkov, and A. Bansemer, 2016: Polarimetric radar and aircraft

observations of saggy bright bands during MC3E. *J. Geophys. Res. Atmos.*, **121**, 3584–3607, https://doi.org/10.1002/2015JD024446.

Löffler-Mang, M., and U. Blahak, 2001: Estimation of the equivalent radar reflectivity factor from measured snow size spectra. *J. Appl. Meteor.*, **40**, 843–849, https://doi.org/10.1175/1520-0450(2001)040<0843:EOTERR>2.0.CO;2.

Luers, J. K., and R. E. Eskridge, 1998: Use of radiosonde temperature data in climate studies. *J. Climate*, **11**, 1002–1019, https://doi.org/10.1175/1520-0442(1998)011<1002:UORTDI>2.0.CO;2.

Miloshevich, L. M., H. Vomel, D. N. Whiteman, and T. Leblanc, 2009: Accuracy assessment and correction of Vaisala RS92 water vapor measurements. *J. Geophys. Res.*, **114**, D11305, https://doi.org/10.1029/2008JD011565.

Politovich, M. K., 1989: Aircraft icing caused by large supercooled droplets. *J. Appl. Meteor.*, **28**, 856–868, https://doi.org/10.1175/1520-0450(1989)028<0856:AICBLS>2.0.CO;2.

——, and T. A. O. Bernstein, 2002: Aircraft icing conditions in northeast Colorado. *J. Appl. Meteor.*, **41**, 118–132, https://doi.org/10.1175/1520-0450(2002)041<0118:AICINC>2.0.CO;2.

Pruppacher, H. R., and J. D. Klett, 1997: *Microphysics of Clouds and Precipitation*. 2nd ed. Atmospheric Sciences Library, Kluwer Academic Publishers, 954 pp.

Rauber, R. M., L. S. Olthoff, M. K. Ramamurthy, and K. E. Kunkel, 2000: The relative importance of warm rain and melting processes in freezing precipitation events. *J. Appl. Meteor.*, **39**, 1185–1195, https://doi.org/10.1175/1520-0450(2000)039<1185:TRIOWR>2.0.CO;2.

——, ——, ——, D. Miller, and K. E. Kunkel, 2001: A synoptic weather pattern and sounding-based climatology of freezing precipitation in the United States east of the Rocky Mountains. *J. Appl. Meteor.*, **40**, 1724–1747, https://doi.org/10.1175/1520-0450(2001)040<1724:ASWPAS>2.0.CO;2.

Reeves, H. D., K. L. Elmore, A. V. Ryzhkov, T. J. Schuur, and J. Krause, 2014: Sources of uncertainty in precipitation type forecasting. *Wea. Forecasting*, **29**, 936–953, https://doi.org/10.1175/WAF-D-14-00007.1.

——, A. V. Ryzhkov, and J. Krause, 2016: Discrimination between winter precipitation types based on spectral-bin microphysics modeling. *J. Appl. Meteor. Climatol.*, **55**, 1747–1761, https://doi.org/10.1175/JAMC-D-16-0044.1.

Ryzhkov, A. V., P. Zhang, H. Reeves, M. Kumjian, T. Tschallener, S. Tromel, and C. Simmer, 2016: Quasi-vertical profiles—A new way to look at polarimetric radar data. *J. Atmos. Oceanic Technol.*, **33**, 551–562, https://doi.org/10.1175/JTECH-D-15-0020.1.

Sand, W. R., W. A. Cooper, M. K. Politovich, and D. L. Veal, 1984: Icing conditions encountered by research aircraft. *J. Climate Appl. Meteor.*, **23**, 1427–1440, https://doi.org/10.1175/0733-3021-23.10.1427.

Stewart, R. E., 1984: Deep 0°C isothermal layers within precipitation bands over southern Ontario. *J. Geophys. Res.*, **89**, 2567–2572, https://doi.org/10.1029/JD089iD02p02567.

Vaisala, 2010: Vaisala radiosonde RS92 performance in the WMO intercomparison of high quality radiosonde systems. Vaisala White Paper, 17 pp. http://www.vaisala.com/Vaisala%20Documents/White%20Papers/WEA-MET-WMO-Test-White_Paper-B211129EN-D-LOW.pdf.

Van den Broeke, M. S., D. M. Tobin, and M. R. Kumjian, 2016: Polarimetric radar observations of precipitation type and rate from the 2–3 March 2014 winter storm in Oklahoma and Arkansas. *Wea. Forecasting*, **31**, 1179–1196, https://doi.org/10.1175/WAF-D-16-0011.1.

Waugh, S. M., 2016: A balloon-borne particle size, imaging, and velocity probe for in situ microphysical measurements. Ph.D dissertation, University of Oklahoma, 189 pp., https://shareok.org/handle/11244/45407.

——, C. L. Ziegler, D. R. MacGorman, S. E. Fredrickson, D. W. Kennedy, and W. D. Rust, 2015: A balloonborne particle size, imaging, and velocity probe for in situ microphysical measurements. *J. Atmos. Oceanic Technol.*, **32**, 1562–1580, https://doi.org/10.1175/JTECH-D-14-00216.1.

Willis, P. T., and A. J. Heymsfield, 1989: Structure of the melting layer in mesoscale convective system stratiform precipitation. *J. Atmos. Sci.*, **46**, 2008–2025, https://doi.org/10.1175/1520-0469(1989)046<2008:SOTMLI>2.0.CO;2.

Zerr, R. J., 1997: Freezing rain: An observational and theoretical study. *J. Appl. Meteor.*, **36**, 1647–1661, https://doi.org/10.1175/1520-0450(1997)036<1647:FRAOAT>2.0.CO;2.